Journal of Alloys and Compounds 501 (2010) 307–312

Contents lists available at ScienceDirect

Journal of Alloys and Compounds

journal homepage: www.elsevier.com/locate/jallcom

Local distortion in Co-doped LSMO from entropy-maximized charge density distribution

K.S. Syed Ali [a], R. Saravanan [a,*], A.V. Pashchenko [b], V.P. Pashchenko [b]

[a] Department of Physics, The Madura College, Madurai 625011, India
[b] Galkin Donetsk Institute of Physics and Technology, National Academy of Sciences of Ukraine, Donetsk 83114, Ukraine

ARTICLE INFO

Article history:
Received 18 December 2009
Received in revised form 7 April 2010
Accepted 14 April 2010
Available online 22 April 2010

Keywords:
Ceramics
Solid state reaction
Crystal structure
X-ray diffraction

ABSTRACT

Perovskite structure manganites $La_{0.67}Sr_{0.22}Mn_{1.11-x}Co_xO_3$ were prepared by the solid state reaction method. An X-ray analysis of the structure was undertaken using the Rietveld technique on the experimental powder X-ray diffraction data and, then, a charge density distribution study was undertaken, using the maximum entropy method (MEM). The charge density in the unit cell was reconstructed and the effect of Co^{3+} doping in the Mn–O matrix was studied. Local distortions due to Co doping were analyzed and the results are now discussed.

1. Introduction

In recent years, there have been many research studies of colossal magneto resistance (CMR) effects in rare earth manganite perovskites because of their potential applications [1–3]. The interplay between structure, magnetic properties and transport properties in perovskite-type manganites $La_{1-x}Sr_xMn_{1-x}Co_xO_3$ (where La is the trivalent rare earth ion and Sr is the divalent alkaline ion) has become of intense interest in today's research. These materials expose many interesting effects, such as magnetoresistance, magnetocaloric, charge, orbital and spin ordering, and elastic properties, etc. [4–6]. More and more researchers are investigating the critical behavior of transition metal-doped LSMO materials [7–12].

In perovskite structures, the MnO_6 octahedra (six Mn–O bonds) are formed by connecting Mn with six corner oxygen atoms, forming a 3-D network. Since the electronic and magnetic interactions occur via Mn(3d)–O(2p)–Mn(3d) paths, the structures of these MnO_6 octahedra (e.g., bond lengths and Mn–O–Mn bond angle) represent information that is important for an understanding of the electronic and physical properties [13]. These compounds are Mn^{3+} and Mn^{4+} rich and doping of divalent atoms introduces mixed valency of Mn^{3+} and Mn^{4+} ions, which plays a major role in double-exchange (DE) ferromagnetic interaction when coupled with metallic resistivity. However, it has been claimed that an additional mechanism, Jahn–Teller distortion (JT), could be responsible for the transport properties [14]. In some compounds, there is a real space ordering of the charge carrier in certain orbitals, resulting from lattice distortion and coulomb correlation of electrons. Orbital ordering manifests itself in site-dependent orientation of the quadrupole moment, as a result of the spatial distribution of the outermost valence d-electrons. As the magnetic and transport properties are closely correlated to the orbital and charge degrees of freedom, there have been many efforts to clarify the microscopic mechanisms that give rise to these exotic phenomena.

The substitution of La^{3+} ions by Sr^{2+} results in a transition from an antiferromagnetic insulating state to a ferromagnetic metallic state with a Mn^{3+}–O^{2-}–Mn^{4+} mixed valence state that is responsible for the mobile charge carriers. At the same time, the substitution of Co doping for Mn can bring T_C to room temperature and also suppresses the double-exchange ferromagnetism and metallic conduction [15]. The Jahn–Teller distortion removes the double-degeneracy of Mn d-electrons in e_g orbitals and provides a mechanism for strong coupling among the electronic, magnetic and lattice degrees of freedom.

However, the doping effect of Co in place of Mn in $La_{1-x}Sr_xMn_{1-x}Co_xO_3$ and its properties are not well known. Mixing the transitional metal elements changes the complete ordering behavior of orbitals and, hence, makes the compound more interesting. When Co is doped in place of Mn, the resultant Co-doped LSMO material exhibits magnetic behavior that is important to explore [12,13]. The present analysis, using powder XRD, determines the effects of Co doping in Mn host lattice by Rietveld

* Corresponding author. Tel.: +91 452 2673354.
E-mail address: saragow@dataone.in (R. Saravanan).
URL: http://www.saraxraygroup.net/ (R. Saravanan).

0925-8388/$ – see front matter © 2010 Elsevier B.V. All rights reserved.
doi:10.1016/j.jallcom.2010.04.093

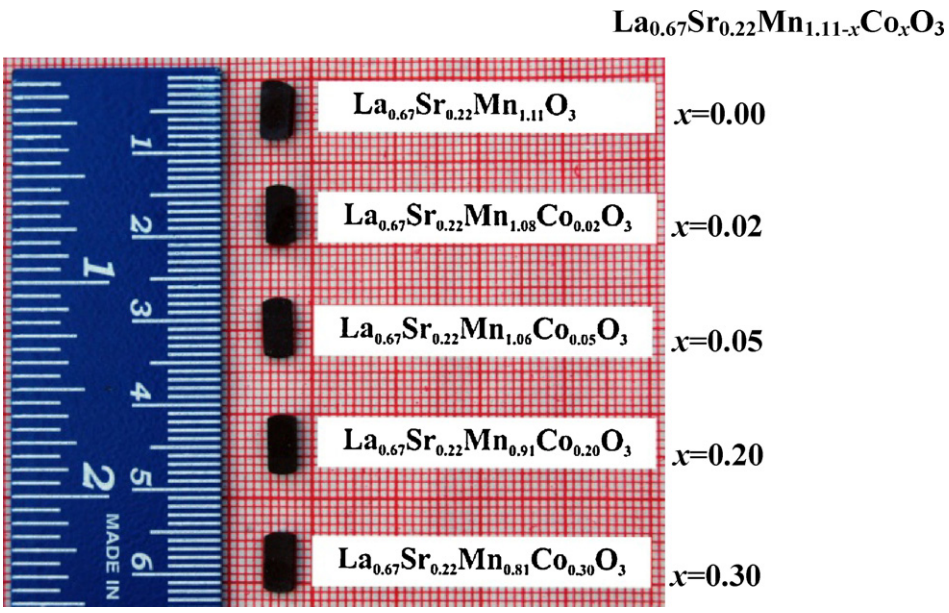

Fig. 1. The grown sample of $La_{0.67}Sr_{0.22}Mn_{1.11-x}Co_xO_3$ (x = 0.00, 0.02, 0.05, 0.20 and 0.30).

analysis and charge density distribution using the maximum entropy method (MEM). Investigating $La_{0.67}Sr_{0.22}Mn_{1.11-x}Co_xO_3$ in the present work is important because Co has a special spin state that is associated with the need to reveal the specific features of the conducting state of the material.

2. Preparation of the samples

Ceramic samples of $La_{0.67}Sr_{0.22}Mn_{1.11-x}Co_xO_3$ were prepared by the standard solid state reaction method [16,17] of appropriate mixing of $La(OH)_3$ (99.9%), $SrCO_3$ (99%), Mn_3O_4 (99.99%) and Co_3O_4 (99.99%) powders and annealing the mixture at a temperature of 900 °C for 20 h and then at 950 °C for a further 20 h. The prepared materials were ground, pressed, and sintered at a temperature of 1350 °C for 21 h, followed by slow cooling. Fig. 1 shows the actual grown samples of $La_{0.67}Sr_{0.22}Mn_{1.11-x}Co_xO_3$ with x = 0.0, 0.02, 0.05, 0.2, and 0.3. For the most part, the grown ceramic samples contain perovskite. The sizable composition of the resultant material is found to contain Mn_3O_4.

2.1. Rietveld refinement

The X-ray powder data sets were collected using a monochromatic incident beam of Cu Kα radiation on an X-PERT-PRO (Philips, Netherlands) X-ray diffractometer, with 2θ ranging from 10° to 120°. The crystal structure was refined by Rietveld analysis [18], using the Jana2006 [19] software program. The crystal structure of the $La_{0.67}Sr_{0.22}Mn_{1.11-x}Co_xO$ was refined in the hexagonal setting with 6 unit formulas per unit cell. The initial crystal structure parameters were those given by Paiva Santos et al. [20]. In the hexagonal setting, La and Sr are fixed at the 6a site (0, 0, 0.25), Mn is fixed at 6b (0, 0, 0) and O is at the 18e site (x, 0, 0.25), with x being refined, starting at a value of 0.5. Starting from refining the lattice parameter along with the shift parameter, the background was trimmed, using as many as 15 terms in a Legendre polynomial function. The profile was constructed using a pseudo-Voigt function [21] that employs a combination of Gaussian and Lorentzian profile functions. Profile asymmetry is introduced by employing the multi-term Simpson rule integration devised by Howard [22] that incorporates a symmetrical profile shape function with different coefficients for weights and peak shift. The La, Sr and Mn, Co occupancies were refined and found to contain 0.67 of La, 0.22 of Sr and 1.11 of Mn at the 6a site and x amount of Co at the 6b site for all of the compounds prepared. The isotropic displacement parameter B_{iso} for all atoms was refined, along with other parameters. A surface roughness correction was also applied using the Pitschke, Hermann and Matter [23] model. Fig. 2(a)–(e) show the Rietveld refined profile for $La_{0.67}Sr_{0.22}Mn_{1.11-x}Co_xO_3$ and Table 1 shows the refined structural parameters. The percentage of Mn_3O_4 was found to vary between 9.03 and 10.08%. It is inferred that, as the concentration of Co increases, the concentration of additional phase Mn_3O_4 decreases. This may be due to the fact that the Co addition to the host lattice has been done properly using solid state reaction to reduce the Mn_3O_4 phase. The Mn_3O_4 compound is found to be of the tetragonal type with $I4_1/amd$ with atomic positions of Mn as (0, 0, 0) and O as (−0.5, 0, −0.25). The extra peaks found in the original profile were found to match those of the secondary phase (i.e., Mn_3O_4). The refined profiles show both sets of Bragg peaks as vertical lines for the primary and secondary phases as bottom and top vertical lines, respectively. The Rietveld [18] fittings reveal a nice matching of the observed and calculated profiles for all of the five systems. The phase fraction of the composition was found to contain almost 90% of the primary phase and 10% of the secondary phase. The cell parameters obtained in this work by Rietveld [18] refinement yielded consistent cell values and are presented in Table 1.

3. Charge density from maximum entropy method (MEM)

As for the LSMO material, many researchers have concentrated mainly on the magnetic behaviour of the material and the surface level characterization [4–6]. In this work, we have concentrated on the electronic image reconstruction from the charge density evaluated from X-ray structure factors simple because the magnetic and electrical conducting behaviors depend more on the arrangement of charges and their involvement in the bonding process.

The origin of charge ordering can be understood from the accurate electronic structure inside the unit cell. This can be achieved by constructing the charge density from X-ray structure factors using the best possible mathematical tool, such as the maximum entropy method (MEM). This method was successfully introduced in X-ray crystallography to construct charge density in the unit cell

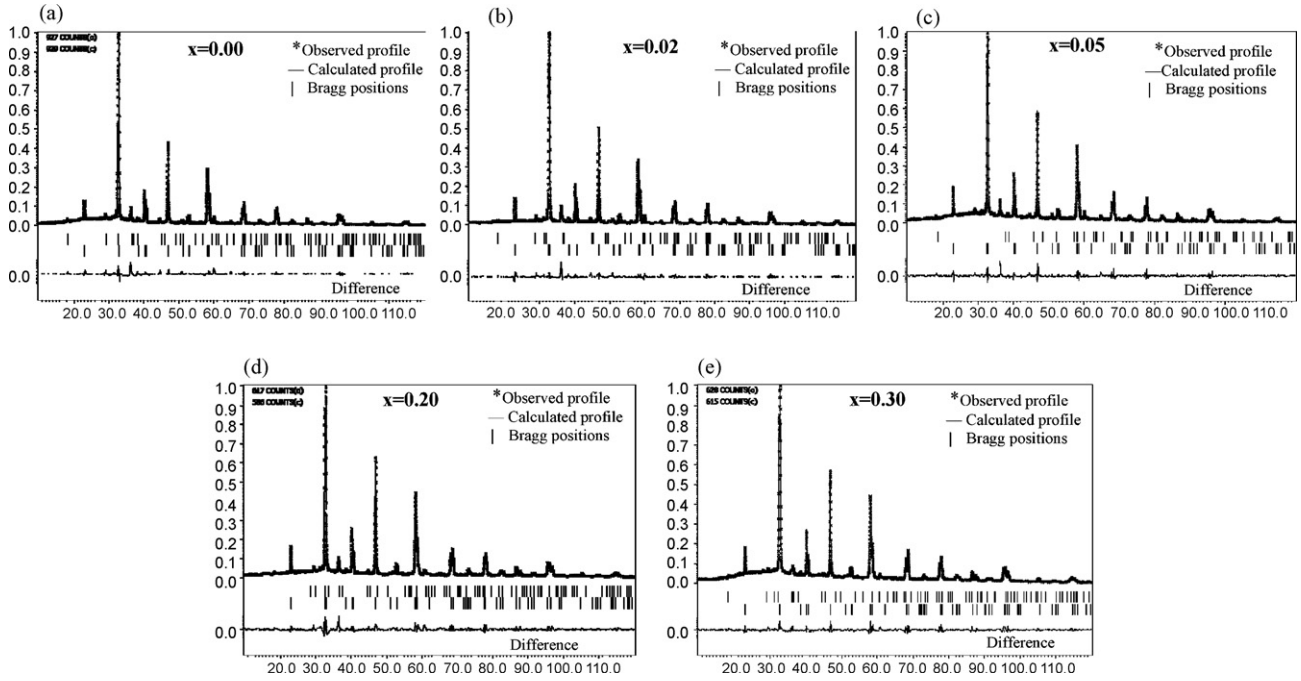

Fig. 2. (a) Rietveld refined profile for $La_{0.67}Sr_{0.22}Mn_{1.11-x}Co_xO_3$ at (a) $x = 0.00$, (b) $x = 0.02$, (c) $x = 0.05$, (d) $x = 0.20$, (e) $x = 0.30$.

Table 1
Structural parameters from Rietveld refinement of powder XRD data of $La_{0.67}Sr_{0.22}Mn_{1.11-x}Co_xO_3$.

Parameter	$x = 0.00$	$x = 0.02$	$x = 0.05$	$x = 0.20$	$x = 0.30$
a (Å)	5.5709(535)	5.5895(5)	5.5238(73)	5.4543(57)	5.4115(21)
c (Å)	13.5141(736)	13.5675(15)	13.3960(25)	13.2159(96)	13.1051(51)
Cell volume (Å^3)	363.23(4)	367.12(6)	353.98(2)	340.49(7)	332.36(5)
B_{La} (Å^2)	0.6446(459)	0.5836(39)	0.6780(753)	0.5856(32)	0.7792(542)
B_{Mn} (Å^2)	1.9780(279)	1.7719(547)	1.8625(96)	2.2679(831)	1.5588(732)
B_O (Å^2)	2.2218(863)	0.9388(127)	0.8094(235)	0.7112(54)	1.0426(124)
x (O)[a]	0.541(7)	0.538(6)	0.531(9)	0.527(7)	0.524(8)
R_{obs} (%)	2.22	2.39	2.16	2.92	2.79
wR_{obs} (%)	2.67	2.88	2.33	3.02	2.91
R_p (%)	11.43	10.44	12.83	13.72	11.03
wR_p (%)	13.02	12.63	12.47	14.22	12.99

[a] Refinable fractional coordinate x of O atom.

by Collins [24] in 1982. MEM infers electron densities in such a way that they provide the maximum variance of structure factors, $Fc_{(MEM)}$, within errors in observed structural factors $\sigma(F_o)$. MEM gives very accurate and less noisy density maps than does a Fourier synthesis [25].

In the present work, the charge density is computed using the PRIMA software [26], which employs the MEM technique. The resultant density is plotted with the help of VESTA visualization software [27]. The detailed methodology of MEM analysis is presented in Syed Ali et al. [28]. The parameters involved in the present analysis are presented in Table 2. The 3-D charge density distribution constructed using the MEM model is presented with similar iso surface levels in the unit cell, along with a ball and stick model of the structure as Fig. 3(a)–(e). In the crystal structure of $La_{0.67}Sr_{0.22}Mn_{1.11-x}Co_xO_3$, the lanthanum atom is coordinated by nine oxygen atoms and the Mn atom by six oxygen atoms, forming irregular octahedra. These figures correspond to the charge density of $La_{0.67}Sr_{0.22}Mn_{1.11-x}Co_xO_3$ ($x = 0.00$, 0.02, 0.05, 0.20, 0.30) materials.

Table 2
Parameters from the MEM analyses of $La_{0.67}Sr_{0.22}Mn_{1.11-x}Co_xO_3$.

Parameter	$x = 0.00$	$x = 0.02$	$x = 0.05$	$x = 0.20$	$x = 0.30$
Number of cycles	361	214	294	226	375
Prior density, $\tau(r_i)$ (e/Å^3)	0.4008	0.4457	0.4718	0.4654	0.4590
Lagrange parameter (λ)	0.0093	0.0184	0.0183	0.0179	0.0125
R_{MEM} (%)	0.92	1.31	1.27	1.29	1.33
wR_{MEM} (%)	0.11	1.38	1.51	1.46	1.43

It is understood from the report of Hu et al. [16] that the magnetoresistance in $La_{0.67}Sr_{0.33}Mn_{1-x}Co_xO_3$ occurs at the Curie temperature $T_C = 362$ K (for $x = 0.0$), which is higher than room temperature. By substituting Co for Mn, it is possible to decrease T_C to room temperature. For example, T_C is 323 K for $x = 0.08$ and 315 K for $x = 0.1$, respectively [16]. The substitution of Co for Mn is known to greatly affect electronic transport behavior. Also, room temperature resistivity in a zero field rises with Co substitution for Mn in $La_{0.67}Sr_{0.33}Mn_{1-x}Co_xO_3$, reflecting the reduction in the metal conductivity. The Co substitution also effectively destroys Mn^{3+}–O^{2-}–Mn^{4+} bonds and reduces the number of electron carriers, suppressing the double-exchange ferromagnetism and metallic conduction [16].

Fig. 3(a)–(e) reveals a unique situation in which the charges extend out from their respective atomic positions to the valence region. The increased Co doping in the Mn site leaves the charges to undergo localized ordering and is illustrated in the Figs. In the MnO_6

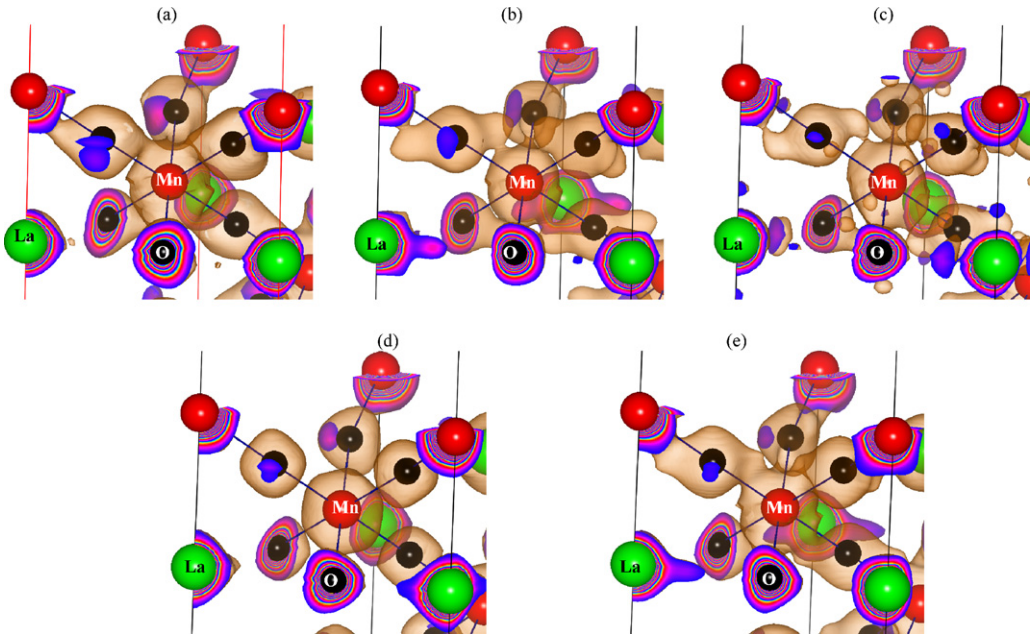

Fig. 3. (a) Charge density of $La_{0.67}Sr_{0.22}Mn_{1.11-x}Co_xO$ in the unit cell at (a) $x = 0.00$, (b) $x = 0.02$, (c) $x = 0.05$, (d) $x = 0.20$, (e) $x = 0.30$ (iso surface level = 0.25).

octahedra, the oxygen seems to rotate anticlockwise and enters a more strained charge environment and almost detaches ($x = 0.2$) itself from bonding. The strain in the charge reaches a maximum at $x = 0.2$ and decreases thereafter. This could well be the signature of induced ferromagnetism introduced due to charge ordering in the chosen range of doping concentration. Thus, room temperature ferromagnetism in $La_{0.67}Sr_{0.22}Mn_{1.11-x}Co_xO_3$ is understandably due to the implantation of Co^{3+} in the MnO matrix, as evident by the charge density pictures.

In Fig. 3(a)–(e), it can be seen that the implantation of the Co^{3+} ion actually reduces the size of the Mn^{3+} ions and also decreases the charge density at the atomic site of Mn^{3+} (the ionic radii for Mn^{3+} and Co^{3+} are 0.67 and 0.65 Å, respectively, and the ionic radii for La^{3+} and Sr^{2+} are 1.16 and 1.26 Å, respectively [29]). The contribution of Co^{3+} to the MnO matrix seems to have strengthened the ionic character in the system. This confirms an increase in the resistivity with the substitution of Co in the MnO matrix as observed by Hu et al. [16]. Thus, charge density gives the right responses to the behavior of the chosen system when Co is substituted in it.

To quantify these results, we have plotted 2-D maps and 1-D profiles along the investigating bonding directions. In Fig. 4(a)–(e) the contribution of Co^{3+} to the Mn–O matrix seems to have strengthened the ionic character in the system, as indicated by the depletion of charge density in the valence region. The fact that the covalent

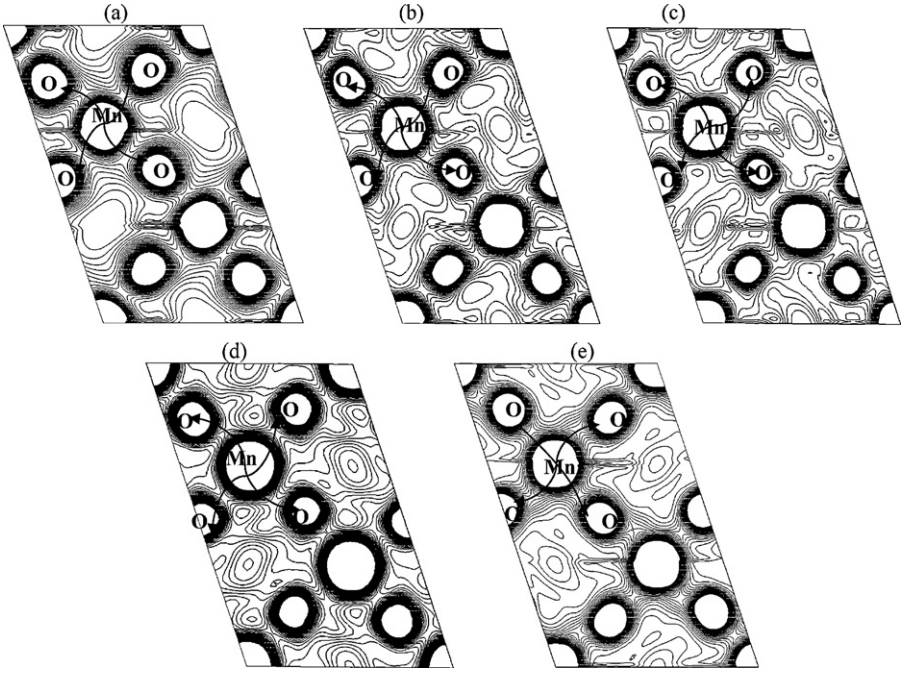

Fig. 4. (a) 2-D MEM electron density distribution of $La_{0.67}Sr_{0.22}Mn_{1.11-x}Co_xO$ on the (0 1 2) plane for (a) $x = 0.00$, (b) $x = 0.02$, (c) $x = 0.05$, (d) $x = 0.20$, (e) $x = 0.30$ (contour range is from 0.00 to 1.0 e/Å^3. Contour interval is 0.03 e/Å^3).

Table 3
MEM electron density in valence region between Mn–O.

x	Mn–O	
	Distance (Å)	Density (e/Å^3)
0.00	1.0266	0.2281
0.02	1.0852	0.1938
0.05	1.1737	0.1837
0.20	1.0814	0.1693
0.30	1.0536	0.2802

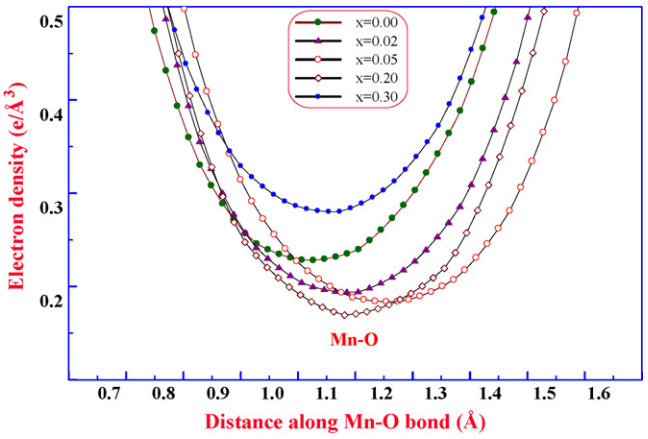

Fig. 5. One-dimensional variation of electron density along [Mn–O] bonding direction.

and ionic radii of the Co element are less than their Mn counterparts and the difference between the electronegativity of the Mn and Co ions is very small add to the fact that the implantation of Co^{3+} can induce the system's insulating behavior. The result shows that, when Co ions are doped, the size of the Mn atom is reduced and, hence, the mid-bond region becomes charge-depleted and exhibits more closed shell interaction. This is proven by the lower charge density at the mid-bond points between Mn and O (Table 3). These events can confirm that the reduction of metallicity due to Co doping in the chosen sample. Fig. 4(a)–(e) shows that the charge density returns to its original state after going through a full cycle of charge ordering as when $x = 0$. The magnitude of the valence charges can be quantified by understanding the 1-D charge density profiles drawn along the bonding direction.

The 1-D charge density variation plotted between Mn–O as shown in Fig. 5 clearly indicates that the substitution of Co for Mn affects the electronic transport behavior. The mid-bond density decreases with increasing Co substitution up to $x = 0.2$ and then increases at $x = 0.3$. Thus, the mid-bond density between Mn and O atoms strongly suggests that the insulating behavior in the chosen system occurs only between $x = 0.0$ and 0.2 and then the system reverts to its original state. This behavior also has a telling effect on the system's ferromagnetic behavior in the region where $x = 0.0$–0.2.

The investigation of the Jahn–Teller distortion in this compound is very interesting. For the purpose, we have used charge density as a tool to explain and confirm the presence of the Jahn–Teller effect in the chosen system. The Jahn–Teller effect causes any non-linear molecules in a degenerate electronic state to have a displacement of nuclei along at least one non-totally symmetric normal coordinate. This gives rise to a distortion of molecular geometry with a concomitant decrease in energy. It has been very difficult to understand the behavior both computationally and experimentally. Hence, it remains a real challenge.

Due to the measurement time frame, the Jahn–Teller effect does not allow the distortion to be seen because of molecules moving randomly or because the distortion is so small as to be negligible. Hence, freezing a molecule to slow the distortion in the latter case is not possible. Still, it may be possible if the structure is solved using low temperature X-ray data. However, the lattice distortion, along with the hopping of electrons between the manganese atoms causes the charge density of oxygen to adopt the unique charge geometry that is observed in our work. The charge density of oxygen goes into a spiraling geometry as the substitution of Co increases in the lattice. This causes the bond path to bend in the way that is shown in Fig. 4(a)–(e). This indicates that the substitution of Co enhances electron transport, thereby introducing more distortion in the octahedral cage of oxygen atoms and also reducing the symmetry. It is our understanding that the depletion of charges along the bond path is primarily due to the transfer of charges that enhance the insulating behavior, although this is introduced here because of the spiraling geometry of the charge density of the oxygen atom. The rotation of oxygen is complete at $x = 0.2$ and the bond detaches (see Fig. 3(d)) and, hence, the increase in the strain in the lattice. It is observed that, at a higher percentage of Co doping (i.e., at $x = 0.3$), the bonds realign themselves so as to have more charges between the Mn and O atom and, thus, the strain decreases to the original state. This behavior suggests that the Jahn–Teller distortion introduced to the system is due to the strain in the charge imparted by the Co doping in the MnO matrix. This strain also causes the Mn–O distance to increase between $x = 0.02$ and 0.2 and then lessen. However, the mid-bond density assumes its lowest

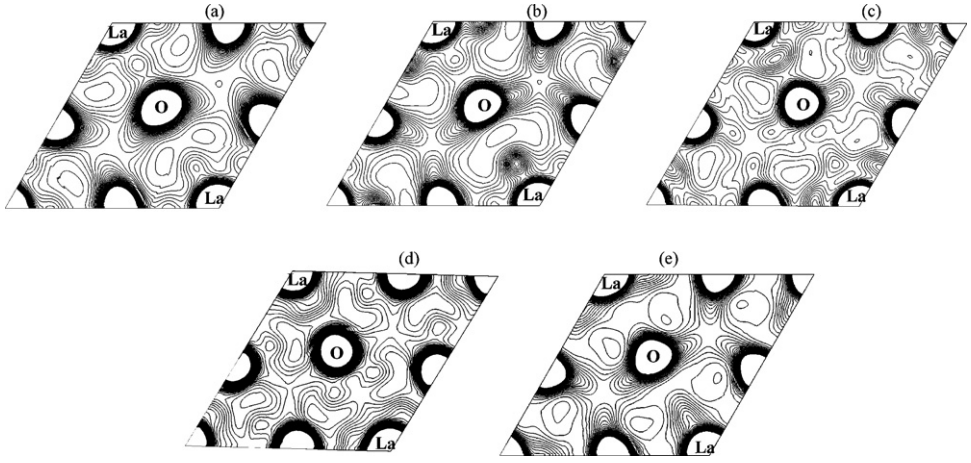

Fig. 6. (a) 2-D MEM electron density distribution of $La_{0.67}Sr_{0.22}Mn_{1.11-x}Co_xO$ on the (0 0 4) plane for (a) $x = 0.00$, (b) $x = 0.02$, (c) $x = 0.05$, (d) $x = 0.20$, (e) $x = 0.30$ (contour range is from 0.00 to 1.0 e/Å^3. Contour interval is 0.03 e/Å^3).

value at $x = 0.2$, also indicating that the Jahn–Teller distortion is greater at this point.

The Jahn–Teller distortion also affects the La–O bond as explained in Fig. 6(a)–(e). These pictures (Fig. 6(a)–(e)) show that, due to the geometrical rotation of the charge density of O, more charge is accumulated between La and O. This accumulation of charge increases from $x = 0$ to 0.05 and then decreases sharply at $x = 0.3$. The previous discussion of the La–O bond and the mid-bond charge between La and O completely complements the effect of distortion in the Mn–O bond.

4. Conclusions

The precise local structure and bonding in $La_{0.67}Sr_{0.22}Mn_{1.11-x}Co_xO_3$ has been studied using versatile methods, such as the Rietveld analysis and the maximum entropy method (MEM) using powder X-ray data. In the Rietveld analysis, we have found that 9.03% of additional phase (Mn_3O_4) is present along with the host. A charge density analysis was conducted for the title compounds and the charge ordering was investigated to deduce their electrical and structural properties.

Acknowledgements

On behalf of the authors of this article, Dr. R. Saravanan expresses appreciation to the Council of Scientific and Industrial Research (CSIR) for its financial assistance to the research project No.: 03(1138)/09/EMR-II.

References

[1] Y.C. Liang, Y.C. Liang, J. Cryst. Growth 304 (2007) 275.
[2] S.P. Liu, G.D. Tang, P. Hao, L.Q. Xu, Y.G. Zhang, W.H. Qi, X. Zhao, D.L. Hou, W. Chen, J. Appl. Phys. 105 (2009) 013905.
[3] E.S. Bozin, M. Schmidt, A.J. DeConinck, G. Paglia, J.F. Mitchell, T. Chatterji, P.G. Radaelli, T. Proffen, S.J.L. Billinge, Phys. Rev. Lett. 98 (2007) 137203.
[4] R.I. Zainullina, N.G. Bebenin, V.V. Ustinov, Y.M. Mukovskii, J. Alloys Compd. 467 (2009) 22.
[5] H.S. Im, G.B. Chon, S.M. Lee, B.H. Koo, C.G. Lee, M.H. Jung, J. Magn. Magn. Mater. 310 (2007) 2668.
[6] D.T. Hanh, M.S. Islam, F.A. Khan, D.L. Minh, N. Chau, J. Magn. Magn. Mater. 310 (2007) 2826.
[7] R.V. Wandekar, B.N. Wani, S.R. Bharadwaj, Solid State Sci. 11 (2009) 240.
[8] A. Ben Amora, M. Koubaa, W. Cheikhrouhou-Koubaa, A. Cheikhrouhou, J. Alloys Compd. 467 (2009) 78.
[9] C.P. Yang, S.S. Chena, D.H. Guoa, H. Wanga, G.H. Raob, V. Morchshakov, K. Barner, J. Alloys Compd. 467 (2009) 54.
[10] I.T. Gomes, B.G. Almeida, A.M.L. Lopes, J.P. Araújo, J. Barbosa, J.A. Mendes, J. Magn. Magn. Mater. 322 (9–12) (2010) 1174.
[11] R.K. Gupta, E.Y. Kim, Y.H. Kim, C.M. Whang, J. Alloys Compd. 490 (1–2) (2010) 56.
[12] G.V. Bazuev, A.V. Korolyov, M.A. Melkozyorova, T.I. Chupakhina, J. Magn. Magn. Mater. 322 (5) (2010) 494.
[13] T. Shibata, B.A. Bunker, J.F. Mitchell, Phys. Rev. B 68 (2003) 024103.
[14] N. Sundarum, Y. Jiang, I.E. Anderson, D.P. Belanger, C.H. Booth, F. Bridges, J.F. Mitchell, T. Proffen, H. Zheng, Phys. Rev. Lett. 102 (2009) 026401.
[15] L.V. Bau, N.V. Khiem, N.X. Phuc, L.V. Hong, D.N.H. Nam, P. Nordblad, J. Magn. Magn. Mater. 322 (6) (2010) 753.
[16] J. Hu, H. Qin, J. Chen, R.K. Zheng, J. Appl. Phys. 91–10 (2002) 8912.
[17] X.G. Li, X.J. Fan, G. Ji, W.B. Wu, K.H. Wong, C.L. Choy, H.C. Ku, J. Appl. Phys. 85–3 (1999) 1663.
[18] H.M. Rietveld, J. Appl. Crystallogr. 2 (1969) 65.
[19] V. Petříček, M. Dušek, L. Palatinus, Jana2006, The Crystallographic Computing System, Institute of Physics Academy of Sciences of the Czech Republic, Praha, 2000.
[20] C.O. Paiva Santos, R.F.C. Marques, M. Jafelicci Jr., L.C. Varanda, Powder Diff. 17–2 (2002) 149.
[21] W.I.F. David, J. Appl. Crystallogr. 19 (1986) 63.
[22] C.J. Howard, J. Appl. Crystallogr. 15 (1982) 615.
[23] W. Pitschke, H. Hermann, N. Mattern, Powder Diff. 8–2 (1993) 74.
[24] D.M. Collins, Nature 49 (1982) 298.
[25] L.B. McCusker, R.B. Von Dreele, D.E. Cox, D. Louër, P. Scardi, J. Appl. Crystallogr. 32 (1999) 36.
[26] A.D. Ruben, I. Fujio, Super-fast Program PRIMA for the Maximum-Entropy Method, Advanced Materials Laboratory, National Institute for Materials Science, 1-1 Namoki, Tsukuba, Ibaraki, Japan 305 (2004) 0044.
[27] K. Momma, F. Izumi, Commission Crystallogr. Comput. IUCr Newslett. 7 (2006) 106.
[28] K.S. Syed Ali, R. Saravanan, S. Israel, R.K. Rajaram, Bull. Mater. Sci. 29–2 (2006) 107.
[29] http://www.smisoftware.com/Html/PeriodicTable/index.htm.